

Van der Waals–Casimir–Polder interaction of an atom with a composite surface

E. Eizner¹, B. Horovitz¹, and C. Henkel^{2, a}

¹ Physics Department, Ben Gurion University of the Negev, Beer Sheva, Israel

² Institute of Physics and Astronomy, University of Potsdam, Germany

Received 7 May 2012 / Received in final form 17 July 2012

Published online (Inserted Later) – © EDP Sciences, Società Italiana di Fisica, Springer-Verlag 2012

Abstract. We study the dispersion interaction of the van der Waals and Casimir–Polder (vdW-CP) type between a neutral atom and the surface of a conductor by allowing for nonlocal electrodynamics, i.e. electron diffusion. We consider two models: (i) bulk diffusion, and (ii) diffusion in a surface charge layer. In both cases, we find that the transition to a semiconductor as a function of the conductivity is continuous, unlike the case of a local model. The relevant parameter is the electric screening length and depends on the carrier diffusion constant. We find that for distances comparable to the screening length, vdW-CP data can distinguish between bulk and surface diffusion, hence it can be a sensitive probe for surface states.

1 Introduction

Recent progress in the understanding of the van der Waals–Casimir–Polder (vdW-CP) force between an atom and a surface allows by now to distinguish surface properties with respect to charge transport. Data on the temperature and atom-surface distance dependence provide excellent tools for such analysis. In particular the experiments on fused silica [1,2] have demonstrated a temperature dependence of the vdW-CP interaction. Fused silica is considered as a dilutely doped semiconductor that has a finite conductivity σ . The data was fitted successfully to the potential for a dielectric surface which differs from the one for a perfectly reflecting mirror, as considered by Casimir and Polder [3]. In fact, since σ/ω diverges at zero frequency, any nonzero conductivity will reproduce the perfect reflector result [4]. It has been suggested to resolve this puzzle with the help of a nonlocal model of the electromagnetic response, where charge diffusion and screening become essential at low conductances [5], although the approach was met with criticism [6,7]. In a related experiment on the (macroscopic) Casimir force between a gold-coated sphere and a single-crystal silicon membrane [8], the results are consistent with a dielectric behavior in its pristine form (ignoring the σ/ω tail). The significant change in the charge carrier density after laser illumination leads to a metallic response in local form, again in agreement with Casimir force measurements. Nonlocal theories have been worked out to understand the crossover between these limits [5,9–11], although experimental data favor a local description where the contribution of free charge carriers is omitted in the

dielectric state [6–8]. For the discussion whether nonlocal electrodynamics may be applied to macroscopic Casimir interactions, and its consistency with thermodynamics, see references [6,7,12–15,17].

The ability of probing charge transport may provide for an increased understanding of surface science by using the vdW-CP interaction as a probe. This viewpoint may be traced back to the seminal paper by Zaremba and Kohn [18] where the van der Waals potential (neglecting retardation) was calculated with a microscopic description of the many-electron response of a metal. Their analysis yields an expression for the reference plane with respect to which the atom-surface distance z is actually calculated. See reference [19] for a review of related methods. Dorofeyev [20] analyzed the van der Waals (non-retarded) regime with the help of a nonlocal (k -dependent) electromagnetic response based on the surface impedance work by Kliewer and Fuchs [21]; the electrons were assumed to reflect specularly from the inner surface.

In the present work, we compare two non-local models that can be understood as mesoscopic extensions of the work by Zaremba and Kohn [18]: (i) the first one allows for bulk diffusion as in references [5,9], we denote it “continuous charge” (CC). In the non-retarded limit, this reduces to the Kliewer and Fuchs approach [21] for a hydrodynamic dielectric function in the bulk. The model (ii) allows for diffusion only within a surface layer (“charge layer” or CL), the bulk charges responding with a local conductivity. Such composite surfaces with charges in the bulk and on the surface, are fairly common in metallic systems. These surfaces are either covered with adsorbates or nanostructures and can, e.g., be used as sensitive chemical sensors and biosensors [22], or are disordered with

^a e-mail: Carsten.Henkel@physik.uni-potsdam.de

quantum well states at the surface [23]. Further motivation for a two-type charge model comes from studies of the anomalous heating of cold ions observed in miniaturized Paul traps that invoke surface charge fluctuations on the metallic electrodes [24–28]. Composite surfaces have also been explored regarding surface plasmons and lead to a wide range of dispersion relations, as observed in different systems, see reference [29] and references therein.

The hallmark of the non-local theory is charge diffusion. In the CC model, it is described by the diffusion coefficient D in the bulk, while D_s describes surface diffusion in the CL. We identify a screening length a_0 (cgs units)

$$a_0 = \sqrt{\frac{\epsilon_\infty D}{4\pi\sigma}}, \quad a_0 = \sqrt{\frac{\epsilon_\infty D_s}{4\pi\sigma}}, \quad (1)$$

where σ, ϵ_∞ are the bulk conductivity and background dielectric constant, respectively. As the atom-surface distance z becomes comparable to the length scale a_0 , the vdW-CP interaction changes its behaviour. We consider different materials where a_0 can be compared with the other two important length scales of the vdW-CP potential: the radiation wavelength $\lambda_A = c/\Omega$, Ω being the atomic transition frequency, and the thermal photon wavelength $\lambda_T = \hbar c/k_B T$ at temperature T . As common for electric dipole transitions in the visible range, we assume here $\lambda_A \ll \lambda_T$, but explore otherwise the full range of distances. After defining the charge models (Sect. 2), we study in Section 3 the case that a_0 is in the van der Waals (short distance) regime, $a_0 \ll \lambda_A$, focusing on the $T = 0$ case. In Section 4, the length a_0 is in the Casimir-Polder (intermediate) regime, $\lambda_A \ll a_0 \ll \lambda_T$, while in Section 5 we consider long distances $a_0 \gg \lambda_T$ where screening affects the Lifshitz (thermal) regime of the interaction. In all these cases we find that the crossover from the vdW-CP potential for a local conductor to a dielectric occurs at $z \approx a_0$. In addition, the dispersion interaction is a good surface probe in the sense that the crossover is different in the CC and CL systems. This difference is particularly visible when the two limits, metallic and dielectric, are well separated. The relevant parameters are discussed in the conclusion.

2 Model

2.1 Atom–surface interaction potentials

We use in this paper the general formulation of Wylie and Sipe [30,31] for the Casimir-Polder potential of an atom with a surface. Assuming the surface and the electromagnetic field in equilibrium at temperature T , the free energy of interaction is given by

$$\mathcal{F}(\mathbf{r}) = -k_B T \sum_{l=0}^{\infty} \sum'_{ij} \alpha_{ij}(i\xi_l) G_{ji}(\mathbf{r}, \mathbf{r}; i\xi_l), \quad (2)$$

which is a sum over Matsubara frequencies $\xi_l \equiv 2\pi l k_B T / \hbar$ along the imaginary frequency axis. The primed sum is

taking the $l = 0$ term with a factor $\frac{1}{2}$. The atomic polarizability $\alpha_{ij}(\omega)$ is given in equation (4) below, the retarded Green tensor $G_{ij}(\mathbf{r}, \mathbf{r}; \omega)$ is made explicit in equations (6) and (7). In the limit $T \rightarrow 0$, \mathcal{F} reduces to the interaction energy

$$U(\mathbf{r}) = -\frac{\hbar}{2\pi} \int_0^\infty d\xi \sum_{ij} \alpha_{ij}(i\xi) G_{ji}(\mathbf{r}, \mathbf{r}; i\xi). \quad (3)$$

This formulation applies for an atom in the ground state, for which the polarizability tensor is given by

$$\alpha_{ij}(\omega) = \lim_{\eta \rightarrow 0^+} \frac{2}{\hbar} \sum_e \frac{\Omega_{eg} d_i^{ge} d_j^{eg}}{\Omega_{eg}^2 - (\omega + i\eta)^2}, \quad (4)$$

where Ω_{eg} is the transition frequency between the ground state (g) and an excited state (e) with an electric dipole matrix elements $g \leftrightarrow e$ and $d_i^{ge} = \langle g | d_i | e \rangle$. We focus on a single resonance and assume rotational symmetry, so that $\Omega_{eg} = \Omega$ and the polarizability is isotropic, $\alpha_{ij} = \alpha \delta_{ij}$.

The electromagnetic Green tensor $G_{ij}(\mathbf{r}, \mathbf{r}'; \omega)$ in equation (2) provides the electric field $E_i(\mathbf{r})$ radiated by a test dipole located at \mathbf{r}' and oscillating with amplitude d_j at frequency ω :

$$E_i(\mathbf{r}) = \sum_j G_{ij}(\mathbf{r}, \mathbf{r}'; \omega) d_j. \quad (5)$$

For a source outside a polarizable body, this electric field can be calculated within macroscopic electrodynamics (see, e.g., Refs. [30,31]) and involves the reflection (or scattering) amplitudes of the body. It turns out that these amplitudes are sufficient to determine the Casimir-Polder interaction. The subtraction of the free-space part of the Green tensor (Lamb shift) is understood in the following. At a planar surface, only two principal polarizations $p = \text{TM}, \text{TE}$ are relevant, and the reflection amplitudes depend on frequency and a wave vector k parallel to the surface $r_p = r_p(\omega, k)$. As we put $\mathbf{r} = \mathbf{r}'$ in equations (2) and (3), the planar symmetry implies that the Green tensor is diagonal with elements [30,31] (cgs units)

$$G_{xx}(\mathbf{r}, \mathbf{r}; \omega) = \int_0^\infty dk \frac{k e^{-2v_0 z}}{2v_0} \left[v_0^2 r_{\text{TM}} + \frac{\omega^2}{c^2} r_{\text{TE}} \right] \quad (6)$$

$$G_{zz}(\mathbf{r}, \mathbf{r}; \omega) = \int_0^\infty dk \frac{k^3 e^{-2v_0 z}}{v_0} r_{\text{TM}}, \quad (7)$$

the element G_{yy} being identical to G_{xx} . The vacuum decay constant for a field mode with frequency ω and parallel wave vector k is

$$v_0 = \sqrt{k^2 - \omega^2/c^2}, \quad (8)$$

with the root chosen such that $\text{Re } v_0 \geq 0$ and $\text{Im } v_0 \leq 0$. The reflection amplitudes are collected in Table 1 for the different surface models considered in this paper.

The general equation (2), valid for any T , now takes the form

$$\begin{aligned} \mathcal{F}(z) = & -\frac{k_{\text{B}}T}{2} \int_0^\infty dk 2k^2 e^{-2kz} \alpha(0) r_{\text{TM}}(0, k) \\ & - k_{\text{B}}T \sum_{l=1}^\infty \alpha(i\xi_l) \int_0^\infty dk \frac{k}{v_0} e^{-2v_0z} \left[2k^2 r_{\text{TM}}(i\xi_l, k) \right. \\ & \left. + \frac{\xi_l^2}{c^2} (r_{\text{TM}}(i\xi_l, k) - r_{\text{TE}}(i\xi_l, k)) \right]. \end{aligned} \quad (9)$$

Let us briefly recall the assumptions behind the Wylie and Sipe approach [30,31]: the interaction energy is calculated in perturbation theory with respect to the atom-field coupling, starting from a well-defined atomic level (here, the ground state). The temperature provides Boltzmann weights for the excited states of the electromagnetic field, thus including the interaction with blackbody radiation and its modification by the surface. The thermal population of excited states of the atom is negligible provided the Bohr frequency is large enough, $\hbar\Omega \gg k_{\text{B}}T$. Otherwise, a temperature-dependent polarizability should be used in equations (2) and (9). Finally, the surface response is worked out ignoring the presence of the atom and assuming a linear response of the surface to electromagnetic radiation, consistent with common practice in surface spectroscopy. By inspection of equation (9), one notes that wave vectors up to $k \sim 1/z$ are relevant for the interaction potential. At distances z much larger than the size of the unit cell, a macroscopic treatment of the surface response is therefore justified. There have been discussions what kind of electromagnetic response may be used consistently for atom-surface potentials and macroscopic Casimir interactions in general, see references [6,7,12–15,17]. The approach of references [30,31] is based on the fluctuation-dissipation theorem [32].

2.2 Surface response with charge diffusion

Surfaces covered with thin layers of strongly localized charges or adsorbates have been studied in much detail in surface physics. For a general theory of their electromagnetic response, see references [33,34]. We consider here a model introduced in reference [26] where the surface is covered by a charge sheet with a charge density $\gamma(x, y)$ (localized in the plane $z = 0$). The details of the electromagnetic response are worked out in Appendix. The sheet current in the layer responds by diffusion

$$\mathbf{J} = -D_s(\omega) \nabla_{\parallel} \gamma, \quad (10)$$

where $D_s(\omega) = D_s/(1 - i\omega\tau_s)$ is the surface diffusion coefficient and τ_s a surface relaxation time. The gradient appearing here is parallel to the layer. A surface conductivity term proportional to \mathbf{E} is neglected, as justified for a small layer thickness, see Appendix A.3. Charge conservation yields

$$-i\omega\gamma + \nabla \cdot \mathbf{J} = j_z(0^-), \quad (11)$$

so that the bulk current just below the layer, $j_z(0^-)$, provides the influx into the surface layer. We take the bulk current response in the usual Ohmic form

$$z < 0: \quad \mathbf{j} = \sigma(\omega) \mathbf{E}, \quad (12)$$

where the Drude conductivity is $\sigma(\omega) = \sigma/(1 - i\omega\tau)$ with a scattering time τ . Equations (10) and (12) define the CL (charge layer) model.

The CC (continuous charge) model, in contrast, is defined by the bulk charge density that has a diffusion constant D , i.e. equation (12) is replaced by

$$\mathbf{j} = \sigma(\omega) \mathbf{E} - D(\omega) \nabla \rho. \quad (13)$$

The “additional” boundary condition for the current is then $j_z(0^-) = 0$, since there are no surface charges in this nonlocal model.

The resulting reflection amplitudes are summarized in Table 1 and more details on their derivation are given in Appendix. One notes that the TE polarization is not affected by the composite structure of the surface. This can be understood from the fact that surface charges are created by electric fields perpendicular to the surface, which are absent in this polarization.

To illustrate the impact of the diffusive layer, we have calculated the local photonic mode density, i.e., the imaginary part of $G_{ii}(\mathbf{r}, \mathbf{r}; \omega)$. This quantity can be measured from the spontaneous decay rate of an excited atom placed at \mathbf{r} or from the heating rate of an ion trapped near a surface [24–28]. The results shown in Figure 1 illustrate the enhancement of the mode density at low frequencies (below the characteristic scale $D_{(s)}/z^2$, left column). At large wave vectors (short distances, right column), there is a competition between additional modes (enhancing the mode density, CL model) and screening (reducing it, CC model). Note that for the parameters considered here the screening length a_0 is much smaller than the diffusion length $\sim \sqrt{D_{(s)}/\omega}$. An excited atom decays faster because diffusion along the surface broadens the field spot it creates, increasing the effective area where absorption takes place. Calculations of the Casimir (plate-plate) interaction between materials with a nonlocal electromagnetic response have revealed qualitatively similar trends (compare Refs. [35,36] to Ref. [37]). The experimental data of reference [8] are better described with a local rather than nonlocal theory, however, see reference [15] and the discussion in references [16,17].

3 Van der Waals (nonretarded) regime

This regime corresponds to short distances where retardation is negligible

$$z \ll \lambda_A \equiv c/\Omega, \quad (14)$$

with a typical value $\lambda_A \approx 100$ nm for transitions in the visible range. The Van der Waals interaction follows a power law $\mathcal{F}(z) \sim 1/z^3$ for a material with a local response (Drude metal or dielectric). We consider in this

Table 1. The reflection coefficients $r_{\text{TE}}(\omega, k)$ and $r_{\text{TM}}(\omega, k)$ for two models for a nonlocal surface response. Symbols used: The dielectric function $\epsilon(\omega)$ is defined at equation (18) while $\epsilon_s(\omega, k)$ is defined at equation (17). Spatial decay rates are for the vacuum $v_0(\omega, k)$, equation (8), for transverse fields in the medium $v(\omega, k) = \sqrt{k^2 - \epsilon(\omega)\omega^2/c^2}$ with $\text{Re } v > 0$ and for compressional charge waves $v_1(\omega, k) = \sqrt{k^2 - i\omega\epsilon(\omega)/[\epsilon_\infty D(\omega)]}$ with $\text{Re } v_1 > 0$ and $D(\omega) = D/(1 - i\omega\tau)$.

	Local	Hydrodynamic bulk charge (CC)	Charge layer (CL)
$r_{\text{TE}}(\omega, k)$	$\frac{v_0 - v}{v_0 + v}$	$\frac{v_0 - v}{v_0 + v}$	$\frac{v_0 - v}{v_0 + v}$
$r_{\text{TM}}(\omega, k)$	$\frac{\epsilon v_0 - v}{\epsilon v_0 + v}$	$\frac{\epsilon v_0 - v - (\epsilon - \epsilon_\infty) \frac{k^2}{\epsilon_\infty v_1}}{\epsilon v_0 + v + (\epsilon - \epsilon_\infty) \frac{k^2}{\epsilon_\infty v_1}}$	$\frac{\epsilon_s v_0 - v}{\epsilon_s v_0 + v}$

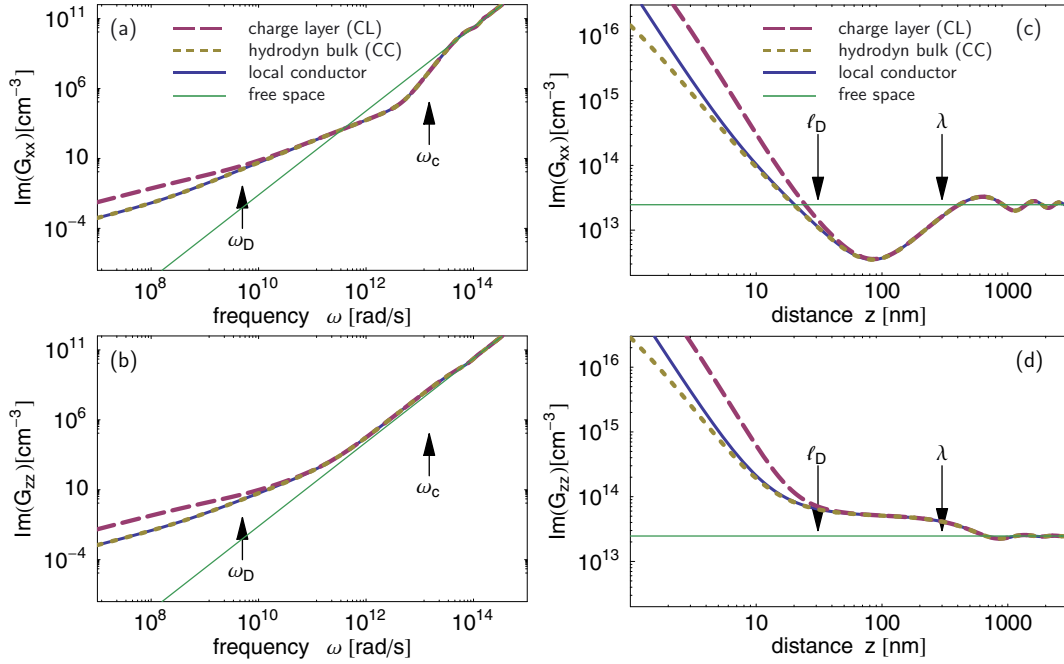


Fig. 1. (Color online) (a, b) Local photonic mode density near a metallic surface, described as a local Ohmic conductor (solid blue curves), by a continuous bulk charge (CC) model (dotted yellow curves, superimposed), and a diffusive charge layer (CL) model (dashed purple curves). Thin green lines: free space mode density. We plot the imaginary part of the Green functions in equations (6) and (7); top row: polarization parallel to surface (G_{xx}), bottom row: perpendicular polarization (G_{zz}). Parameters: conductivity $\sigma = 3.6 \times 10^{17}$ rad/s, typical for Al, relaxation time $\tau = \tau_s = 10^{-15}$ s, diffusion constant $D_s = D = 5 \times 10^3$ cm²/s, background permittivity $\epsilon_\infty = 1$, giving a screening length $a_0 \approx 0.3$ nm, and distance $z = 10 \mu\text{m}$. The plots include the free space response that provides the dominant $\sim \omega^3$ scaling at high frequencies. Characteristic diffusion frequency for these parameters: $\omega_D = D/z^2 = 5 \times 10^9$ rad/s (left arrow); right arrow: inverse photon round trip time $\omega_c = c/(2z)$. (c, d) Distance dependence of the local mode density near a metallic surface, described by the same models as in the left column. Same parameters, except that the frequency is fixed to $\omega = 10^{15}$ rad/s (near-infrared). The plots include the free space response, that leads to a constant limit $\frac{2}{3}\omega^3$ at large distance (thin horizontal lines). The oscillations are due to partial standing waves formed above the surface. Diffusion length for these parameters: $\ell_D = \sqrt{2D/\omega} \approx 31$ nm (left arrow); right arrow: reduced wavelength $\lambda = c/\omega$.

section the situation that the screening length (see Introduction) satisfies $a_0 \ll \lambda_A$; this corresponds to electron densities typical for metals.

We start from the zero-temperature expression for the interaction potential, combining equations (3), (4), (6), (7):

$$U(z) = -\frac{\hbar}{2\pi} \int_0^\infty d\xi \alpha(i\xi) \int_0^\infty dk \frac{k}{v_0} e^{-2v_0 z} \left[2k^2 r_{\text{TM}}(i\xi, k) + (\xi^2/c^2)(r_{\text{TM}}(i\xi, k) - r_{\text{TE}}(i\xi, k)) \right] \quad (15)$$

where now $v_0^2 = k^2 + \xi^2/c^2$. The dominant ranges of the integrals are around $k \sim 1/z \gg \Omega/c$, due to the exponential, and $\xi \leq \Omega$, due to the polarizability $\alpha(i\xi)$. This allows to simplify equation (15) by taking $\xi \ll ck$ and $v_0 \approx k$, so that for the CL model (see Tab. 1)

$$U(z) \approx -\frac{\hbar\alpha(0)}{\pi} \int_0^\infty d\xi \frac{\Omega^2}{\xi^2 + \Omega^2} \times \int_0^\infty dk e^{-2kz} k^2 \frac{\epsilon_s(i\xi, k)k - v}{\epsilon_s(i\xi, k)k + v}. \quad (16)$$

The reflection amplitude involves a “surface dielectric function” given by (see Ref. [26] and Appendix)

$$\epsilon_s(\omega, k) = \epsilon_\infty + \frac{4\pi i\sigma}{(\omega + iD_s(\omega)k^2)(1 - i\omega\tau)}, \quad (17)$$

where $D_s(\omega)$ is the surface diffusion coefficient (see Eq. (10)). The conventional Drude dielectric function (local), with a bulk relaxation time τ and a high-frequency asymptote ϵ_∞ , is

$$\epsilon(\omega) = \epsilon_\infty + \frac{4\pi i\sigma}{\omega(1 - i\omega\tau)}, \quad (18)$$

which happens to be the limiting form of equation (17) when $D_s \rightarrow 0$. From the k -dependence in $\epsilon_s(\omega, k)$, we identify the dimensionless factor $k^2\epsilon_\infty D_s/(4\pi\sigma) = (ka_0)^2$ that defines the screening length a_0 consistent with the definition (1) of the Introduction. For $ka_0 \ll 1$, the reflection amplitude in equation (16) recovers the local behaviour, while at very short distances, $ka_0 \gg 1$, the diffusive (non-local) term dominates. The latter case implies that the conductivity contribution is suppressed in equation (17), leaving only the background dielectric constant ϵ_∞ .

If $\epsilon_\infty > 1$, both limiting cases (conductor and dielectric) show a van der Waals interaction that follows the familiar c_3/z^3 power law, but with different c_3 coefficients. For the dielectric,

$$\text{local diel., } z \ll \lambda_A: \quad U(z) \approx -\frac{\hbar\alpha(0)\Omega}{8z^3} \frac{\epsilon_\infty - 1}{\epsilon_\infty + 1}, \quad (19)$$

while the local Drude conductor gives [30,31]

$$\text{local metal, } z \ll \lambda_A: \quad U(z) \approx -\frac{\hbar\alpha(0)\Omega}{8z^3} \frac{\omega_s}{\Omega + \omega_s}. \quad (20)$$

Here, $\omega_s^2 = 2\pi\sigma/\tau$ is the surface plasmon frequency, and we have neglected Ohmic losses (i.e., $\omega_s, \Omega \gg 1/\tau$). The composite surface models with their nonlocal response give a van der Waals interaction that crosses over between these two limits (see Fig. 3). This is similar to what has been analyzed at large distances by Pitaevskii [5].

We focus here on the somewhat academic case of a simple free-electron metal ($\epsilon_\infty = 1$), where the nonlocal surface response changes even the exponent at short distances because the c_3 coefficient in equation (19) vanishes. To get insight into the small-distance behaviour, we expand the CL reflection coefficient r_{TM} at high momentum and get for $\tau_s = \tau$

$$k \gg \omega_s/c, \xi/c: \quad \frac{\epsilon_s(i\xi, k)k - v}{\epsilon_s(i\xi, k)k + v} \approx \frac{1}{1 + 2(ka_0)^2}. \quad (21)$$

Note that the imaginary frequency ξ drops out in this case, and the suppression $\sim 1/k^2$ on scales shorter than the screening length a_0 . The ξ integral in equation (16) can then be performed, and one gets for $z \ll a_0$ the simple result

$$\text{CL, } z \ll a_0: \quad U(z) \approx -\frac{\hbar\Omega\alpha(0)}{8za_0^2}, \quad (22)$$

instead of the $1/z^3$ power law. The potential then scales only like $\sim 1/z$ because the image charge in or below the surface is smeared over a scale $a_0 \gg z$, as allowed by the finite diffusion constant and by the metallic compressibility. Once $\epsilon_\infty \neq 1$, a non-diffusing image charge at scale z is present, restoring the $1/z^3$ behavior.

In Figure 2, we compare the exact evaluation of the van der Waals potential (15) (dashed curve) to the numerical integration over k of the approximate reflection amplitude (21) (solid gray curve). One gets a good approximation over a wide range of non-retarded distances $0.1 a_0 < z \ll \lambda_A$. Note how the non-local theory matches with the local conductor (solid blue curve) as $a_0 \ll z$.

A similar analysis for the CC model (Tab. 1) yields a screening length $a_0 = \sqrt{\epsilon_\infty D/(4\pi\sigma)}$ involving the bulk diffusion constant, and the approximate form

$$k \sim 1/a_0 \gg \xi/c: \quad r_{\text{TM}}(i\xi, k) \approx \frac{\sqrt{k^2 + 1/a_0^2} - k}{\sqrt{k^2 + 1/a_0^2} + k}. \quad (23)$$

Despite the difference in the reflection amplitudes (Eqs. (21) and (23)), the short-distance asymptote turns out to be just a factor of one half smaller than equation (22) (upper solid gray curve in Fig. 2). These results illustrate the dramatic impact of nonlocal electrodynamics on the van der Waals interaction. We expect them to apply qualitatively in materials where the background polarizability $\epsilon_\infty > 1$ provided by bound electrons is relatively small. The c_3 coefficient in equation (19) is then nonzero, but weak and shifts the short-distance asymptotes of the CL and CC curves in Figure 2 below zero.

4 Casimir-Polder (retarded) regime

This regime corresponds to an intermediate range of distances,

$$\lambda_A \ll z \ll \lambda_T, \quad (24)$$

where the thermal wavelength $\lambda_T = 7.6 \mu\text{m}$ at 300 K. This range is characterized by the form $\mathcal{F} \sim 1/z^4$ for both dielectric and metallic surfaces with a local dielectric response.

For analytic expansions, we consider $T = 0$ so that the ξ -integral of equation (3) still applies. From the exponent $2v_0z$, we read off the characteristic frequency $\omega_c = c/(2z)$ that limits the ξ -integration range to $\xi \lesssim \omega_c$. In the CP regime (24), ω_c is much smaller than the atomic resonance Ω , and we can expand the polarizability

$$\alpha(i\xi) \approx \alpha(0)(1 - \xi^2/\Omega^2). \quad (25)$$

The following discussion applies to a free-electron metal at high density where $\epsilon_\infty = 1$ and $\sigma \gg \Omega$.

4.1 Good conductor

We then have the small parameter ω_c/σ to simplify the reflection coefficients. It turns out that the impact of charge

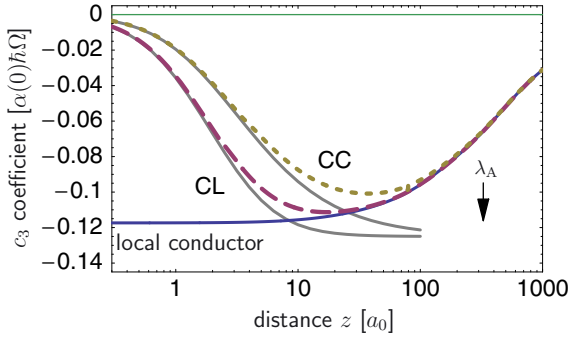


Fig. 2. (Color online) Atom-surface interaction at zero temperature, from the van der Waals into the Casimir-Polder range. We plot the c_3 coefficient, i.e., the potential $U(z)$ multiplied with z^3 , in units of $\hbar\Omega\alpha(0)$. The distance z is in units of the screening length a_0 . The arrow marks the (reduced) transition wavelength λ_A . Solid blue line “local conductor”: Drude metal with dielectric function (18); dashed: surface covered with a diffusive charge layer (CL model); dotted: continuous bulk charge with a hydrodynamic response (CC model). Solid gray lines: short-distance asymptotes to the CL and CC models, based on the approximate reflection coefficients (21, 23). Parameters: DC conductivity $\sigma = 3.6 \times 10^{17} \text{ s}^{-1}$ (typical for Al), dielectric constant $\epsilon_\infty = 1$, electron scattering times $\tau = \tau_s = 10^{-15} \text{ s}$, diffusion constants $D = D_s = 5 \times 10^3 \text{ cm}^2/\text{s}$, atomic resonance wavelength $2\pi\lambda_A = 628 \text{ nm}$ ($\Omega/2\pi = 477 \text{ THz}$). For these parameters, the screening length is $a_0 \approx 0.3 \text{ nm}$. The van der Waals interaction c_3/z^3 with a local Drude conductor gives a normalized value -0.118 from equation (20). The CC/CL models show, at short distances, a much weaker interaction potential $\mathcal{O}(1/z)$ given in equation (22).

diffusion is very small in the Casimir-Polder regime: for the CL model, we find by inspection that the relevant dimensionless ratio is $D_s/(cz) \ll 1$. We start with the zeroth order with respect to this ratio and expand in powers of

$$\delta = \sqrt{\frac{\omega_c}{2\pi\sigma}} \ll 1. \quad (26)$$

Performing the integrations, we get the familiar Casimir-Polder potential and next-order corrections

$$U(z) \approx -\frac{3\hbar c\alpha(0)}{8\pi z^4} \left[1 - \frac{20}{3} \frac{\omega_c^2}{\Omega^2} + \frac{\delta}{6\sqrt{2}} \int_0^\infty dx \sqrt{1 + \omega_c\tau x} \times \left(x^{7/2} \Gamma(0, x) - 3(1+x)e^{-x} x^{3/2} \right) + \mathcal{O}(\delta^2) \right], \quad (27)$$

where the incomplete Gamma function is $\Gamma(0, x) \equiv \int_x^\infty t^{-1} e^{-t} dt$. The limiting values of third term give a correction $-(77/72)\delta\sqrt{\pi/2} \approx -1.34\delta \sim z^{-1/2}$ as $\omega_c\tau \rightarrow 0$ and $-(8/5)\delta\sqrt{2\omega_c\tau} \approx -2.26\delta\sqrt{\omega_c\tau} \sim z^{-1}$ as $\omega_c\tau \rightarrow \infty$.

Note that these approximations correspond to two inequivalent ways of implementing the perfect-conductor limit. The first case could be called “overdamped”, with a purely real conductivity. The penetration of transverse fields into the bulk then occurs by means of diffusion. The

correction to the Casimir-Polder potential in equation (27) scales like $\ell_c/z \propto z^{-1/2}$ where $\ell_c = \sqrt{c^2/\sigma\omega_c}$ is the magnetic diffusion length at the characteristic frequency ω_c . In the second case, the conductivity is purely imaginary and, similar to a superconductor, the transverse field is screened from the bulk. The correction to the Casimir-Polder potential arises from the field penetrating a thin layer of the order of the plasma wavelength (also called London-Meissner penetration depth) $\lambda_p = c\sqrt{\tau/(4\pi\sigma)}$, and scales like λ_p/z . The latter case has been studied, for example, in reference [38], equation (37), and their result is recovered by the two correction terms in equation (27):

$$\frac{U(z) - U_{\text{CP}}(z)}{U_{\text{CP}}(z)} \approx -\frac{5}{3} \frac{\lambda_A^2}{z^2} - \frac{8}{5} \frac{\lambda_p}{z} \quad (\lambda_A \ll z \ll \tau c), \quad (28)$$

where $U_{\text{CP}}(z)$ is the first term in equation (27). This range of distances is quite narrow for the parameters of Figure 2, where $c\tau \approx 300 \text{ nm}$.

Let us now extract the contribution due to the diffusive charge layer (CL model). To the first order in the surface diffusion coefficient D_s , the correction to the local model can be worked out to be:

$$\frac{U(z) - U_{\text{loc}}(z)}{U_{\text{CP}}(z)} \approx -\frac{D_s\delta}{6\sqrt{2}cz} \int_0^\infty dx \frac{\sqrt{x}(1 + \omega_c\tau x)^{1/2}}{1 + \omega_c\tau_s x} \times [e^{-x}(12 + 12x + 3x^2 - x^3) + x^4\Gamma(0, x)]. \quad (29)$$

In the limiting case $\omega_c\tau, \omega_c\tau_s \rightarrow 0$, the integration gives a relative correction $-(285/88)\sqrt{\pi/2}(D_s\delta/cz) \sim z^{-3/2}$; in the opposite limit, $-(12/5)\sqrt{2\tau/\omega_c\tau_s^2}(D_s\delta/cz) = -(6\sqrt{2}/5)(c_s/c)^2(\lambda_p/z)$ where the speed of sound $c_s = \sqrt{D_s/\tau_s}$ characterizes the dispersion of longitudinal modes in the charge layer. The latter estimate illustrates that the correction brought about by the charge layer is negligible in the Casimir-Polder regime. A similar conclusion is reached for the continuous charge (CC) model; we omit the calculations for brevity. The numerical results from Figure 2 illustrate that both CL and CC models merge into the local description in the Casimir-Polder range $z \gtrsim \lambda_A$.

4.2 Semiconductor

Figure 3 shows numerical calculations of the interaction potential for a material with a conductivity typical for semiconductors. The characteristic length a_0 for screening is then much larger and falls into the Casimir-Polder range of the atom-surface potential. The data show that the CC and CL models interpolate between the limiting cases of a local Drude conductor and a non-conducting dielectric (where $\epsilon(\omega) = \epsilon_\infty$ does not diverge at zero frequency). We have taken the relatively low value $\epsilon_\infty = 1.5$ to amplify the difference between the dielectric and the conductor in the local limit: their difference scales with $2/(\epsilon_\infty + 1)$.

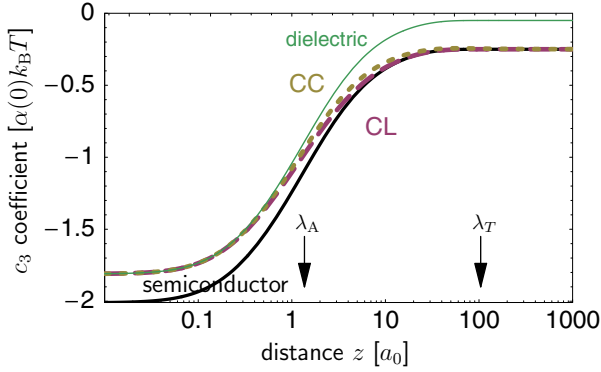


Fig. 3. (Color online) Atom-surface potential through the Casimir-Polder range up to the thermal wavelength. We plot the c_3 coefficient of the free energy, i.e. $\mathcal{F}(z)z^3$, but here in units of $\alpha(0)k_B T$. The distance is normalized to the screening length $a_0 \approx 73$ nm. Solid thick curve: local dielectric function in Drude form; dashed curve: charge layer (CL) model; dotted curve: hydrodynamic (continuous charge, CC) model; solid thin curve: non-conducting local dielectric. Parameters: background dielectric constant $\epsilon_\infty = 1.5$, DC conductivity $\sigma = 10^{10} \text{ s}^{-1}$ (comparable to Ge), electron scattering time $\tau = \tau_s = 10^{-13} \text{ s}$, diffusion constants $D = D_s = 4.5 \text{ cm}^2/\text{s}$, atomic resonance $\Omega/2\pi = 477 \text{ THz}$ (wavelength $2\pi\lambda_A = 628 \text{ nm}$), Temperature $T = 300 \text{ K}$ (thermal wavelength $\lambda_T = 7.6 \mu\text{m}$).

In Figure 3, we show the free energy of interaction $\mathcal{F}(z)$ calculated from the Matsubara sum (9). At distances beyond the thermal wavelength λ_T , the free energy follows a $1/z^3$ power law with a c_3 coefficient proportional to T that we discuss in the following section. The difference between dielectric and Drude conductor arises, for these parameters, from the zeroth term in the Matsubara sum. This term is discussed in more detail in Section 5. Indeed, in the other terms, the conductivity enters only in the ratio $4\pi\sigma/\xi_l = 2\hbar\sigma/(lk_B T)$. At room temperature, this ratio can be neglected compared to the background dielectric constant ϵ_∞ provided the conductivity $\sigma \ll 4 \times 10^{13} \text{ s}^{-1}$. This regime applies to a wide range of doped semi-conductors.

The van der Waals regime for this material is not described by equation (20) due to the low conductivity. Ignoring conductivity completely, equation (19) for a local dielectric gives a short-range coefficient c_3 with a value $-1.91 \alpha(0)k_B T$ in the units of Figure 3: this corresponds well to the full calculation. We have checked that the small difference is actually due to relatively large deviations from the non-retarded approximation that was applied to derive equation (19). A similar situation occurred in reference [39] which discusses the Casimir force between two plates separated by a dielectric liquid.

5 Lifshitz (thermal) regime

This section deals with the long distance regime $\lambda_T \ll z$ where the leading contribution to the atom-surface potential is given by the $l = 0$ term in the Matsubara sum (9). The other terms are proportional to the exponentially small factor $\exp(-4\pi l z/\lambda_T)$ and can be neglected if

the $l = 0$ term is nonzero. A glance at Figure 3 illustrates that the thermal regime is already well borne out at $z \sim \lambda_T$ due to the factor 4π in the exponential.

The static term in the Matsubara sum has been the subject of much discussion in the field of dispersion interactions [40,41]. To illustrate this, we give the limiting forms of the free energy in the thermal range for an ideal dielectric material

$$\lambda_T \ll z: \quad \mathcal{F}(z) \approx -\frac{\alpha(0)k_B T \epsilon_\infty - 1}{4z^3 \epsilon_\infty + 1}, \quad (30)$$

while for a conductor in the same limit

$$\mathcal{F}(z) \approx -\frac{\alpha(0)k_B T}{4z^3}. \quad (31)$$

In fact, the latter result is obtained for any material with a nonzero conductivity: as $\sigma \rightarrow 0$, the former (dielectric) result is not obtained in a continuous manner [4]. This is due to the static reflection coefficient $r_{\text{TM}}(0, k)$ which is equal to 1 for any nonzero σ , while setting $\sigma = 0$ from the start for a pure dielectric, one gets $r_{\text{TM}}(0, k) = (\epsilon_\infty - 1)/(\epsilon_\infty + 1)$. This difference between conductor and dielectric is also visible in the Casimir-Polder range shown in Figure 3. The discontinuity disappears only in the limit $T = 0$ for the material parameters considered here.

This effect is actually an artefact of the description in terms of a local material response (conductivity, dielectric function). Using a hydrodynamic model similar to our CC, Pitaevskii has shown that the free energy shows a continuous cross-over between the limiting cases equations (30) and (31). We show now that the same is true for both CC and CL models considered here.

For the CC model, the first line of equation (9) can be written in terms of a dimensionless integral ($t = 2kz$)

$$\lambda_T \ll z: \quad \mathcal{F}(z) \approx -\frac{\alpha(0)k_B T}{8z^3} \int_0^\infty dt t^2 e^{-t} \frac{\epsilon_\infty \sqrt{t^2 + (2z/a_0)^2} - t}{\epsilon_\infty \sqrt{t^2 + (2z/a_0)^2} + t}, \quad (32)$$

with the screening length a_0 of equation (1). We recover Pitaevskii's result [5] by calculating a_0 from the diffusion coefficient $D \approx k_B T \tau / m^*$ of a non-degenerate electron gas. This leads to $a_0^{-2} = 4\pi n \ell_B$ where n is the carrier density in the conductor and ℓ_B the Bjerrum length (i.e., the distance where the Coulomb energy between two electrons becomes comparable to the thermal energy: $e^2/(\epsilon_\infty \ell_B) = k_B T$). A glance at equation (32) tells that the dielectric and metallic values of the reflection coefficient are smoothly interpolated as the ratio $(z/a_0)^2$ changes from zero to infinity. This is illustrated in Figure 4 (dotted line) where the coefficient of the $1/z^3$ power law is plotted vs z/a_0 .

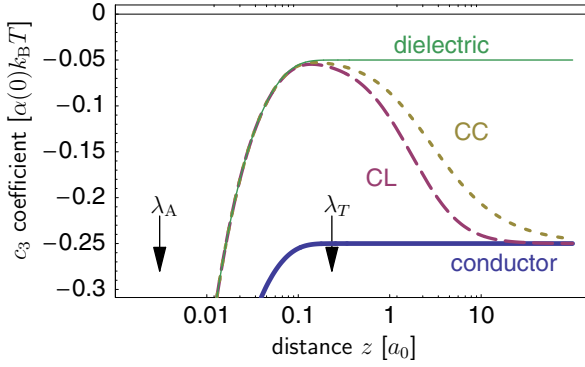


Fig. 4. (Color online) Interaction potential in the thermal range: c_3 coefficient of the free energy, i.e., $\mathcal{F}(z)z^3$, in units of $\alpha(0)k_B T$. The distance is normalized to the screening length $a_0 \approx 33 \mu\text{m}$. Solid thick blue curve: local conductor ($\sigma = 5 \times 10^4 \text{ s}^{-1}$, typical for highly purified water); dashed curve: charge layer (CL) model with diffusion coefficient $D_s = 4.5 \text{ cm}^2/\text{s}$, $\tau_s = 10^{-13} \text{ s}$; dotted curve: continuous bulk charge (CC) model ($D = D_s$, $\tau = \tau_s$); solid thin green curve: ideal dielectric model ($\epsilon_\infty = 1.5$). The other parameters are as in Figure 2.

The same qualitative behaviour is found in the CL model where the free energy takes the form

$$\mathcal{F}(z) \approx -\frac{\alpha(0)k_B T}{8z^3} \int_0^\infty dt t^2 e^{-t} \frac{(\epsilon_\infty - 1)t^2 + \epsilon_\infty(2z/a_0)^2}{(\epsilon_\infty + 1)t^2 + \epsilon_\infty(2z/a_0)^2}. \quad (33)$$

This is shown in dashed in Figure 4. The parameters chosen here are for a very poor conductivity (low carrier density) where the screening length a_0 is large enough to fall into the thermal range. This applies to dilutely doped semiconductors, or to the thermally excited conduction band of an intrinsic semiconductor.

In Figure 5, we explore under which conditions the atom-surface interaction energy is most sensitive to the details of the surface charge response. This contour plot shows the ratio between the CL and CC results for the interaction energy in the thermal range, varying the distance z and the background dielectric constant ϵ_∞ . The two models differ maximally in the crossover range $z \approx a_0$, and for $\epsilon_\infty \sim 1$. This could have been expected from equations (30) and (31) because the dielectric and metallic limits (the two horizontal asymptotes in Fig. 4) are then most separated.

6 Discussion and conclusion

Any material with mobile charges is characterized by a screening length a_0 , and a local current-field relation (Ohm's law) is necessarily limited to scales larger than a_0 . We have explored in this paper how screening at and below the surface influences the long-range van der Waals-Casimir-Polder (vdW-CP) interaction between an atom and the body. Our description may be termed ‘‘mesoscopic’’ in the sense that the electronic response is collective in nature, but retains traces of ballistic carriers via

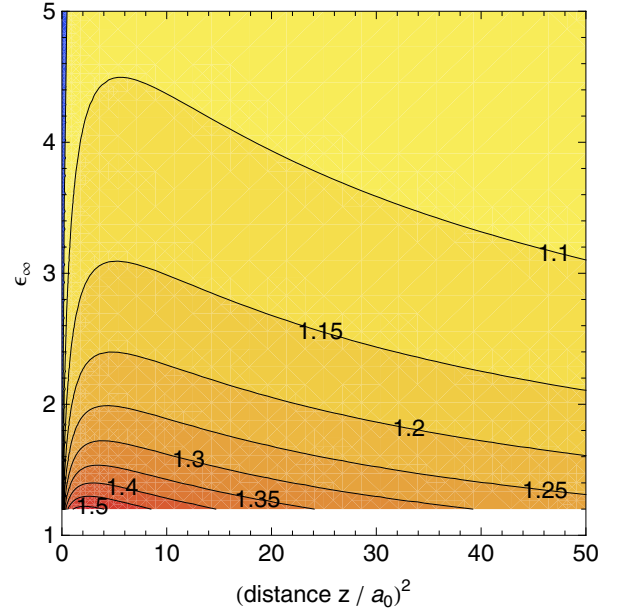


Fig. 5. (Color online) Contour plot of the ratio between the interaction potentials in the CL and CC models. We consider only the thermal range equations (32) and (33). The x -axis gives the ratio $(z/a_0)^2$, the y -axis the background dielectric constant ϵ_∞ . The parameters for surface and bulk diffusion are the same ($D = D_s$, $\tau = \tau_s$).

the diffusion coefficient $D \sim v\ell$ (v is a typical carrier velocity and $\ell = v\tau$ the scattering mean free path). Two models for the electromagnetic response of the surface were studied in detail: a continuous charge distribution below the surface (CC) within a hydrodynamic approximation, and a thin charge layer (CL) with a diffusive response typical for, e.g., localized surface states. Both models provide a continuous crossover of the vdW-CP potential between two local limiting cases: a pure dielectric and a conducting medium, as the atom-surface distance goes through the range $z \sim a_0$. The two limits can be distinguished from the zero-frequency limit of their dielectric functions and give different coefficients c_3 for the $1/z^3$ power laws that prevail at very short (van der Waals) and very large (thermal or Lifshitz) distances. Our calculations extend the picture proposed in references [5,9] to any distances, namely that the nonzero DC conductivity σ can be neglected if the atom-surface distance z is shorter than the screening length a_0 (Eq. (1)).

The differences in the vdW-CP interaction may be used as a probe that can identify the type of charge transport in the (sub)surface region. The sensitivity of this probe is maximal when the screening length a_0 matches the atom-surface distance z , particularly in the retarded range $z > \lambda_A$. The CC/CL difference is particularly large when the dielectric constant ϵ_∞ of bound carriers and background ions is close to 1. The reason is that the jump $\epsilon_\infty - 1$ leads to a surface polarization charge that responds locally (not by diffusion) and is therefore masking the effect of either the CC or the CL. For transitions in the optical visible range, these favorable

conditions correspond to $z > 1 \mu\text{m}$ which is indeed the achievable range of present experiments. A screening length $a_0 \approx 1 \mu\text{m}$ occurs in a dilute semiconductor, which at room temperature is a non-degenerate electron system with $a_0 = \sqrt{\epsilon_\infty k_B T / (4\pi n e^2)}$. Hence we require a carrier density $n \approx 10^{12} \text{cm}^{-3} \times \epsilon_\infty$. This density can be achieved by dilute doping, as for fused silica [5]. One may also work with intrinsic semiconductors where the carriers are thermally excited with a density $n \approx 10^{19} \text{cm}^{-3} \exp(-E_g/2k_B T)$ [9,42] where E_g is the gap. Hence, with $E_g \approx 1 \text{eV}$ and by varying the temperature, one can span a range around 10^{12}cm^{-3} .

In conclusion, our two charge type models are representatives of a composite surface of a metal, with a nonlocal electromagnetic response due to charge transport in the bulk and at the surface. Such composite surfaces are fairly common corresponding to either surfaces covered with adsorbates or nanostructures, or to disordered surfaces with quantum well states. We have studied the Casimir-Polder interaction with such surfaces and have shown where this effect can be used as a sensitive probe of the surface type and its diffusive properties.

This research was supported by a grant from the German-Israeli Foundation for Scientific Research and Development (GIF). We thank H. Haakh for useful discussions and G.L. Klimchitskaya and V.M. Mostepanenko for comment.

Appendix: Surface response

A.1 Surface impedances

The calculation of the electromagnetic Green function proceeds by expanding the field created by a point source into Fourier components and finding reflection and transmission coefficients for each wave vector \mathbf{k}_i incident on the surface. With the wave vector in the xz -plane and the macroscopic body in the half-space $z < 0$, we have $\mathbf{k}_i = k\mathbf{e}_x - k_z\mathbf{e}_z$ with $k_z = \sqrt{\omega^2/c^2 - k^2} = iv_0$. We consider separately two principal polarizations. In the TE-polarization, the electric field outside the surface is written in the form

$$z > 0: \quad \mathbf{E}(\mathbf{r}) = E_{\text{TE}}(k) e^{ikx} \mathbf{e}_y (e^{v_0 z} + r_{\text{TE}} e^{-v_0 z}), \quad (\text{A.1})$$

where \mathbf{e}_y is the unit vector transverse to the plane of incidence. One gets the magnetic field from the Faraday equation: $B_x(\mathbf{r}) = i(c/\omega)\partial_z E_y(\mathbf{r})$. The ratio between these two tangential fields, evaluated at $z = 0^+$, is the surface impedance Z_{TE} and determines the reflection coefficient

$$Z_{\text{TE}} = \frac{E_y(0^+)}{B_x(0^+)}, \quad r_{\text{TE}} = \frac{i(cv_0/\omega)Z_{\text{TE}} - 1}{i(cv_0/\omega)Z_{\text{TE}} + 1}. \quad (\text{A.2})$$

In a local model for the body response, one has $Z_{\text{TE}} = -i\omega/(cv)$ where the transmitted wave vector is $\mathbf{k}_t = k\mathbf{e}_x - i\mathbf{v}\mathbf{e}_z$, and the Fresnel formula is recovered.

In the TM-polarization the electric field vector is in the xz -plane, and equation (A.1) becomes

$$\mathbf{E}(\mathbf{r}) = A_{\text{TM}}(k) e^{ikx} \left[(ik\mathbf{e}_z - v_0\mathbf{e}_x) e^{v_0 z} + r_{\text{TM}}(ik\mathbf{e}_z + v_0\mathbf{e}_x) e^{-v_0 z} \right]. \quad (\text{A.3})$$

This gives $B_y = -i(c/\omega)(\partial_z E_x - ikE_z)$ just above the surface. One defines impedance and reflection coefficient from the tangential (x -) component of the electric field

$$Z_{\text{TM}} = \frac{E_x(0^+)}{B_y(0^+)}, \quad r_{\text{TM}} = \frac{v_0 - i(\omega/c)Z_{\text{TM}}}{v_0 + i(\omega/c)Z_{\text{TM}}}. \quad (\text{A.4})$$

Its local approximation is $Z_{\text{TM}} = -icv/[\omega\epsilon(\omega)]$ where $\epsilon(\omega)$ is the bulk dielectric function.

A.2 Solving the reflection problem

A.2.1 Charge layer model (CL)

We start to work out the electromagnetic response function in the TE-polarization. Within a local description of the bulk medium below the layer, one can work with a medium wave vector \mathbf{k}_t in the xz -plane, as defined after equation (A.2), with

$$iv = \sqrt{(\omega/c)^2 \epsilon(\omega) - k^2}. \quad (\text{A.5})$$

An ansatz similar to equation (A.1) can be written down and augmented by a longitudinal part

$$z < 0: \quad \mathbf{E}(\mathbf{r}) = E_{\text{TE}}(k) e^{ikx} \left[\mathbf{e}_y t_{\text{TE}} e^{vz} + t_L (ik\mathbf{e}_x + v_1\mathbf{e}_z) e^{v_1 z} \right], \quad (\text{A.6})$$

where the component v_1 of the longitudinal wave vector is as yet undetermined. From the Maxwell equations, the tangential component E_x is continuous, and since it is zero above the layer (Eq. (A.1)), we find $t_L = 0$ for the longitudinal amplitude. The field E_z perpendicular to the surface is zero above and below the layer, hence the surface charge γ and the current density \mathbf{J} are zero from equations (10) and (11). The magnetic field B_x is then continuous as well, and we get the local value for the surface impedance from

$$Z_{\text{TE}} = \frac{E_y(0^-)}{B_x(0^-)} = \frac{t_{\text{TE}}}{i(c/\omega)v t_{\text{TE}}}. \quad (\text{A.7})$$

The reflection coefficient (A.2) takes the familiar form

$$r_{\text{TE}} = \frac{v_0 - v}{v_0 + v}. \quad (\text{A.8})$$

In the TM-polarization, both transverse and longitudinal fields in the medium are relevant, as is well known [43]. The expansion (A.6) becomes

$$z < 0: \quad \mathbf{E}(\mathbf{r}) = A_{\text{TM}}(k) e^{ikx} \left[(ik\mathbf{e}_z - v\mathbf{e}_x) t_{\text{TM}} e^{vz} + (ik\mathbf{e}_x + v_1\mathbf{e}_z) t_L e^{v_1 z} \right]. \quad (\text{A.9})$$

The tangential field E_x is continuous and becomes outside the layer

$$E_x(0^+) = A_{\text{TM}}(k) e^{ikx} (-vt_{\text{TM}} + kt_L). \quad (\text{A.10})$$

Due to the surface current density J_x , the field B_y has a jump, and one gets above the layer:

$$\begin{aligned} B_y(0^+) &= B_y(0^-) - \frac{4\pi}{c} J_x \\ &= -i \frac{\omega \epsilon(\omega)}{c} A_{\text{TM}} t_{\text{TM}} + \frac{4\pi}{c} ik D_s(\omega) \gamma. \end{aligned} \quad (\text{A.11})$$

We need to express γ and t_L in terms of the transmitted amplitude t_{TM} : use charge conservation (11) and the continuity of the z -component of the Ampère-Maxwell equation which links the jumps in B_y (surface current) and in ϵE_z (surface charge). A straightforward calculation yields

$$\gamma = -\frac{\sigma(\omega) k A_{\text{TM}} t_{\text{TM}}}{\omega + i D_s(\omega) k^2}, \quad (\text{A.12})$$

and $t_L = 0$. Putting equations (A.10)–(A.12) into equation (A.4), we thus find the impedance

$$Z_{\text{TM}} = \frac{-i(c/\omega)v(1 + i D_s(\omega)k^2/\omega)}{\epsilon(\omega) + i\epsilon_\infty D_s(\omega)k^2/\omega}, \quad (\text{A.13})$$

where ϵ_∞ is the background dielectric function (excluding the conduction current).

A.2.2 Continuous bulk charge model (CC)

The surface impedance in this case is a well-known problem, reviewed in reference [43]. We give some details here for the ease of the reader. An alternative derivation that parallels the argument of the previous paragraph can be found in reference [26].

The CC model is equivalent to the following transverse and longitudinal bulk dielectric functions (relative to the medium wave vector \mathbf{q})

$$\epsilon_\perp(\omega, \mathbf{q}) = \epsilon(\omega) \quad (\text{A.14})$$

$$\epsilon_\parallel(\omega, \mathbf{q}) = \epsilon_\infty + \frac{4\pi i \sigma(\omega)}{\omega + i q^2 D(\omega)}. \quad (\text{A.15})$$

This follows from equation (13) written in Fourier space and using charge conservation in the bulk.

The surface impedances can be found, for example, in the review paper [43], equation (2.26). We assume that the conduction current is tangential to the surface (specular scattering). The impedance in TE-polarization involves only the transverse dielectric function ϵ_\perp , and the reflection coefficient r_{TE} is therefore the same as for a local medium (first row in Tab. 1). With our convention for the reflection coefficients, the TM-impedance is given by

$$\begin{aligned} Z_{\text{TM}} &= -\frac{2i\omega}{\pi c} \int_0^\infty \frac{dq_z}{q^2} \left(\frac{q_z^2}{(\omega/c)^2 \epsilon_\perp(\omega, \mathbf{q}) - q^2} \right. \\ &\quad \left. + \frac{k^2}{(\omega/c)^2 \epsilon_\parallel(\omega, \mathbf{q})} \right), \end{aligned} \quad (\text{A.16})$$

where the dielectric functions are evaluated at the wave vector $\mathbf{q} = k\mathbf{e}_x - q_z\mathbf{e}_z$. Two poles contribute to the integral: a transverse mode at $q^2 = (\omega/c)^2 \epsilon_\perp$ or $q_z = iv$ (Eq. (A.5)), and a longitudinal mode at $\epsilon_\parallel(\omega, \mathbf{q}) = 0$ or $q_z = iv_1$ (Tab. 1). The pole at $q^2 = 0$ does not contribute because its residue vanishes. A straightforward contour integration of equation (A.16) then yields

$$Z_{\text{TM}} = -\frac{ic}{\omega \epsilon(\omega)} \left(v + k^2 \frac{\epsilon(\omega) - \epsilon_\infty}{\epsilon_\infty v_1} \right). \quad (\text{A.17})$$

Inserted into equation (A.4), we get the reflection coefficient r_{TM} given in Table 1.

A.3 Surface conductivity

If we model the charge layer as a film of thickness a and conductivity $\sigma_s(\omega)$, its integrated current density (parallel to the layer) has the form:

$$\mathbf{J}(\mathbf{r}, \omega) = -D_s(\omega) \nabla_\parallel \gamma(x, y) + \sigma_s(\omega) a \mathbf{E}_\parallel, \quad (\text{A.18})$$

where the last term is the conduction current. Including this term in the surface response calculations we get reflection coefficients

$$r_{\text{TM}} = \frac{\epsilon'_s v_0 - v}{\epsilon'_s v_0 + v} \quad (\text{A.19})$$

$$r_{\text{TE}} = \frac{v_0 - v + 4\pi i a \sigma_s(\omega) \omega / c^2}{v_0 + v - 4\pi i a \sigma_s(\omega) \omega / c^2}, \quad (\text{A.20})$$

with the surface dielectric function ϵ'_s being (cf. Eq. (17))

$$\epsilon'_s = \epsilon_\infty + 4\pi i \frac{\sigma(\omega) + va\sigma_s(\omega)}{\omega + i D_s(\omega) k^2}. \quad (\text{A.21})$$

We now identify under which conditions the terms proportional to $\sigma_s(\omega)$ are negligible in these expressions. For an order of magnitude estimate, we take $\sigma_s(\omega) \approx \sigma(\omega)$ and a layer thickness a at the atomic scale. Therefore we get from equation (A.21) the condition

$$va = a \sqrt{k^2 - \frac{\omega^2}{c^2} \epsilon(\omega)} \ll 1. \quad (\text{A.22})$$

An upper limit can be found easily at imaginary frequencies $\omega = i\xi$ where $\epsilon(i\xi) = \epsilon_\infty + 4\pi\sigma/[\xi(1 + \xi\tau)] < \epsilon_\infty + \omega_p^2/\xi^2$, with $\omega_p = \sqrt{4\pi\sigma/\tau}$ the plasma frequency. Using the characteristic scales $k \sim 1/z$ and $\xi \sim \Omega$ in the integrals for the Casimir-Polder potential, the estimate (A.22) becomes

$$a \sqrt{\frac{1}{z^2} + \frac{\epsilon_\infty}{\lambda_A^2} + \frac{1}{\lambda_p^2}} \ll 1. \quad (\text{A.23})$$

Hence we require the layer thickness a to be much smaller than the smallest of the length scales distance z , atomic transition wavelength $\lambda_A = c/\Omega\sqrt{\epsilon_\infty}$ and plasma wavelength $\lambda_p = c/\omega_p$. All these are conditions are well

satisfied for $a \leq 1$ nm. Then the surface dielectric functions ϵ'_s and ϵ_s (Eqs. (A.21), (17)) and the r_{TM} reflection coefficients equation (A.19), Table 1 are equivalent.

As for the r_{TE} amplitude (A.20), we can neglect the surface conductivity term provided

$$\frac{4\pi a \sigma_s(i\xi)\xi}{c^2} \ll \sqrt{\frac{4\pi\sigma(i\xi)\xi}{c^2}} \leq v. \quad (\text{A.24})$$

As an estimate, this is equivalent to

$$\frac{4\pi\sigma a^2\xi}{c^2(1+\tau\xi)} \ll 1. \quad (\text{A.25})$$

The maximal value on the left hand side is $(a/\lambda_p)^2$, hence a must be smaller than the plasma wavelength, as we found before in equation (A.23). In the limit of large k , the difference $v_0 - v$ in equation (A.20) becomes small, and the condition (A.24) must be replaced by

$$\frac{4\pi a \sigma_s(i\xi)\xi}{c^2} \ll \frac{2\pi\sigma(i\xi)\xi}{kc^2}. \quad (\text{A.26})$$

Estimating $k \sim 1/z$, we get $a \ll z$ which we also found in equation (A.23) above. For $a \leq 1$ nm, also the r_{TE} amplitude is therefore not affected by the layer conductivity.

References

1. D.M. Harber, J.M. Obrecht, J.M. McGuirk, E.A. Cornell, Phys. Rev. A **72**, 033610 (2005)
2. J.M. Obrecht, R.J. Wild, M. Antezza, L.P. Pitaevskii, S. Stringari, E.A. Cornell, Phys. Rev. Lett. **98**, 0632019 (2007)
3. H.B. Casimir, D. Polder, Phys. Rev. **73**, 360 (1948)
4. G.L. Klimchitskaya, V.M. Mostepanenko, J. Phys. A **41**, 312002(F) (2008)
5. L.P. Pitaevskii, Phys. Rev. Lett. **101**, 163202 (2008)
6. B. Geyer, G.L. Klimchitskaya, U. Mohideen, V.M. Mostepanenko, Phys. Rev. Lett. **102**, 189301 (2008)
7. L.P. Pitaevskii, Phys. Rev. Lett. **102**, 189302 (2008)
8. F. Chen, G.L. Klimchitskaya, V.M. Mostepanenko, U. Mohideen, Phys. Rev. B **76**, 035338 (2007)
9. D.A.R. Dalvit, S.K. Lamoreaux, Phys. Rev. Lett. **101**, 163203 (2008)
10. V.B. Svetovoy, Phys. Rev. Lett. **101**, 163603 (2008)
11. V.B. Svetovoy, Phys. Rev. Lett. **102**, 219903 (2009), erratum
12. R.S. Decca et al., Phys. Rev. Lett. **102**, 189303 (2009)
13. D.A. Dalvit, S.K. Lamoreaux, Phys. Rev. Lett. **102**, 189304 (2009)
14. Y.S. Barash, V.L. Ginzburg, Sov. Phys. Usp. **18**, 305 (1975)
15. G.L. Klimchitskaya, U. Mohideen, V.M. Mostepanenko, J. Phys. A **41**, 432001 (2008)
16. V.M. Mostepanenko, R.S. Decca, E. Fischbach, B. Geyer, G.L. Klimchitskaya, D.E. Krause, D. Lopez, U. Mohideen, Int. J. Mod. Phys. A **24**, 1721 (2009)
17. L.P. Pitaevskii, Laser Phys. **19**, 632 (2009)
18. E. Zaremba, W. Kohn, Phys. Rev. B **13**, 2270 (1976)
19. J.F. Dobson, T. Gould, J. Phys.: Condens. Matter **24**, 073201 (2012)
20. I. Dorofeyev, Phys. Lett. A **363**, 251 (2007)
21. K.L. Kliever, R. Fuchs, Phys. Rev. **172**, 607 (1968)
22. J. Homola, *Surface plasmon resonance based sensors* (Springer, Berlin, Heidelberg, 2006)
23. A. Varykhalov, A.M. Shikin, W. Gudat, P. Moras, C. Grazioli, C. Carbone, O. Rader, Phys. Rev. Lett. **95**, 247601 (2005)
24. Q.A. Turchette et al., Phys. Rev. A **61**, 063418 (2000)
25. D. Leibbrandt, B. Yurke, R. Slusher, Quant. Inf. Comput. **7**, 52 (2007)
26. C. Henkel, B. Horovitz, Phys. Rev. A **78**, 042902 (2008)
27. R. Dubessy, T. Coudreau, L. Guidoni, Phys. Rev. A **80**, 031402 (2009)
28. N. Daniilidis, S. Narayanan, S.A. Möller, R. Clark, T.E. Lee, P.J. Leek, A. Wallraff, S. Schulz, F. Schmidt-Kaler, H. Häffner, New J. Phys. **13**, 013032 (2011)
29. B. Horovitz, C. Henkel, Europhys. Lett. **97**, 57010 (2012)
30. J.M. Wylie, J.E. Sipe, Phys. Rev. A **30**, 1185 (1984)
31. J.M. Wylie, J.E. Sipe, Phys. Rev. A **32**, 2030 (1985)
32. E.M. Lifshitz, L.P. Pitaevskii, *Statistical Physics*, Part 2 (Pergamon, Oxford, 1980)
33. J.E. Sipe, Phys. Rev. B **22**, 1589 (1980)
34. D. Bedeaux, J. Vlieger, *Optical Properties of Surfaces* (World Scientific, Singapore, 2004)
35. R. Esquivel, V.B. Svetovoy, Phys. Rev. A **69**, 062102 (2004)
36. V.B. Svetovoy, R. Esquivel, J. Phys. A **39**, 6777 (2006)
37. A.M. Contreras-Reyes, W.L. Mochan, Phys. Rev. A **72**, 034102 (2005)
38. V.B. Bezerra, G.L. Klimchitskaya, V.M. Mostepanenko, C. Romero, Phys. Rev. A **78**, 042901 (2008)
39. M. Boström, B.E. Sernelius, I. Brevik, B.W. Ninham, Phys. Rev. A **85**, 010701(R) (2012)
40. B. Geyer, G.L. Klimchitskaya, V.M. Mostepanenko, Phys. Rev. D **72**, 085009 (2005)
41. G.L. Klimchitskaya, U. Mohideen, V.M. Mostepanenko, Rev. Mod. Phys. **81**, 1827 (2009)
42. N.W. Ashcroft, N.D. Mermin, *Solid State Physics* (Saunders, Philadelphia, 1976)
43. G.W. Ford, W.H. Weber, Phys. Rep. **113**, 195 (1984)